Three-dimensional numerical study of global flow effects on interchange instabilities

K. Ichiguchi[1,2], Y. Suzuki[1,2], Y. Todo[1,2], M. Sato[1], K. Ida[1,2], S. Sakakibara[1,2], S. Ohdachi[1,2], Y. Narushima[1,2], B. A. Carreras[3]

[1] *National Institute for Fusion Science, Toki 509-5292, Japan*

[2] *The Graduate University of Advanced Study, SOKENDAI, 509-5292, Japan*

[3] *University Carlos III, Madrid, Spain*

1. Introduction

In the recent experiments in the Large Helical Device (LHD), it is observed that the magnetic perturbation grows rapidly just after the mode rotation stops and causes a partial collapse of the electron temperature[1]. This phenomenon indicates the possibility that the plasma rotation can suppress the growth of the mode. Thus, we numerically study the rotation effects on the MHD stability against the interchange modes in the LHD configuration. As the numerical procedure, we employ a static equilibrium and apply a global shear flow as the rotation to the initial perturbation in the stability calculation. The three-dimensional (3D) numerical codes of HINT[2] and MIPS[3] are utilized for the equilibrium and the stability calculations, respectively. In the original study of the flow effects[4], a model profile is utilized for the flow, and a sample equilibrium that is strongly unstable against the interchange mode is employed. As the result, it is obtained that a sufficiently large flow has a potential to suppress the pressure collapse due to the interchange mode. However, the flow profile is not consistent with the experimental data. Thus, in the present study, the flow profile is improved and is applied to the same sample equilibrium.

2. Calculation of global flow consistent with experimental data

We have established a numerical scheme to calculate the global flow which is consistent with the experimental data[5]. In this scheme, we assume that the flow is stationary, the plasma flows on the magnetic surfaces, and the flow component perpendicular to the magnetic field is given by the ExB flow. Then, the flow is given by

$$v = \hat{V}B + \hat{\Phi}'\nabla\zeta \times \nabla s, \tag{1}$$

in the Hamada coordinates (s, θ, ζ), where s and ζ denote the normalized toroidal magnetic flux and the toroidal angle, respectively. Each factor in eq. (1) is calculated in the following way. The magnetic field B is obtained from the results of the HINT code calculation. The contravariant

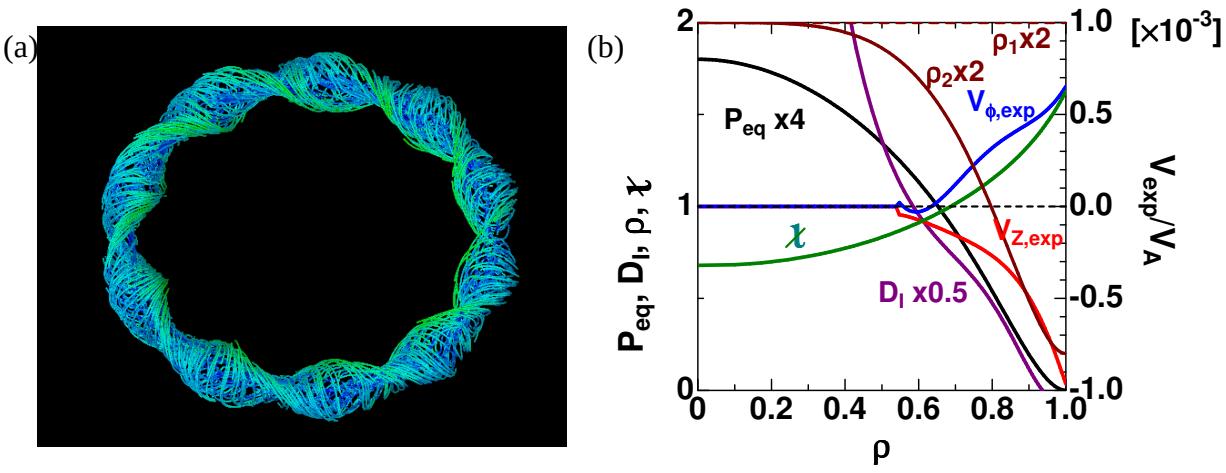

Figure 1: (a) 3D plots of the stream lines corresponding to the flow observed in LHD experiment. (b) Profiles of the flow components in ϕ and Z directions normalized by the Alfvén velocity $v_{\phi,exp}$ and $v_{Z,exp}$, respectively, corresponding to (a), equilibrium pressure P_{eq}, rotational transform ι, and Mercier index D_I. Two types of density profile ρ_1 and ρ_2 are also plotted.

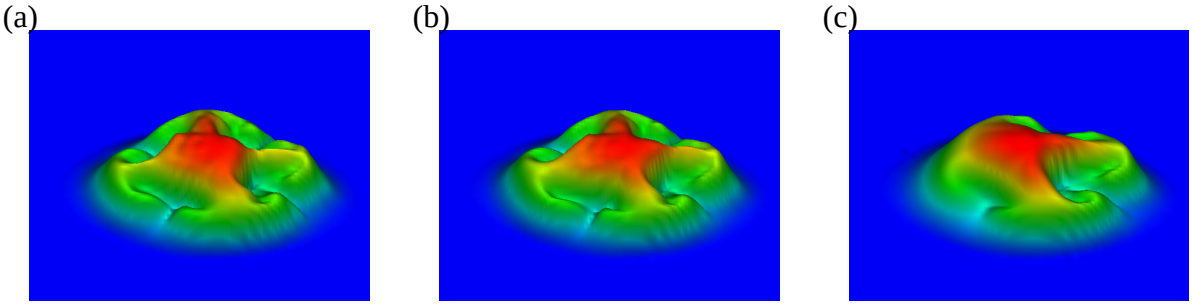

Figure 2: Total pressure profiles with the initial density $\rho_{ini} = \rho_1$ at t=420τ_A for the applied flows of (a) none, (b) $v_{\phi,exp}$ and $v_{Z,exp}$, and (c) $v_{\phi,exp} \times 200$ and $v_{Z,exp} \times 200$.

vector $\nabla\zeta \times \nabla s$ is obtained by means of the surface geometry given by the VMEC code result[6]. The surface quantities $\hat{V}$ and $\hat{\Phi}'$ are calculated with the use of the experimental data.

In LHD, the Z and ϕ components of the flow are observed along the horizontal line in the horizontally elongated cross section, where (R, ϕ, Z) are the cylindrical coordinates. Figure 1 (a) shows a result of the flow calculation. Here, we employ the data observed in a shot showing a pressure collapse. While the flow is observed along a one-dimensional (1D) line in the LHD experiment, this scheme provides the 3D flow profile in the whole plasma region from the data.

3. Effects of global flow on nonlinear dynamics of interchange mode

The effects of the global flow consistent with the experimental data on the dynamics are examined in a sample LHD equilibrium. The equilibrium quantities are shown in Fig.1 (b). The

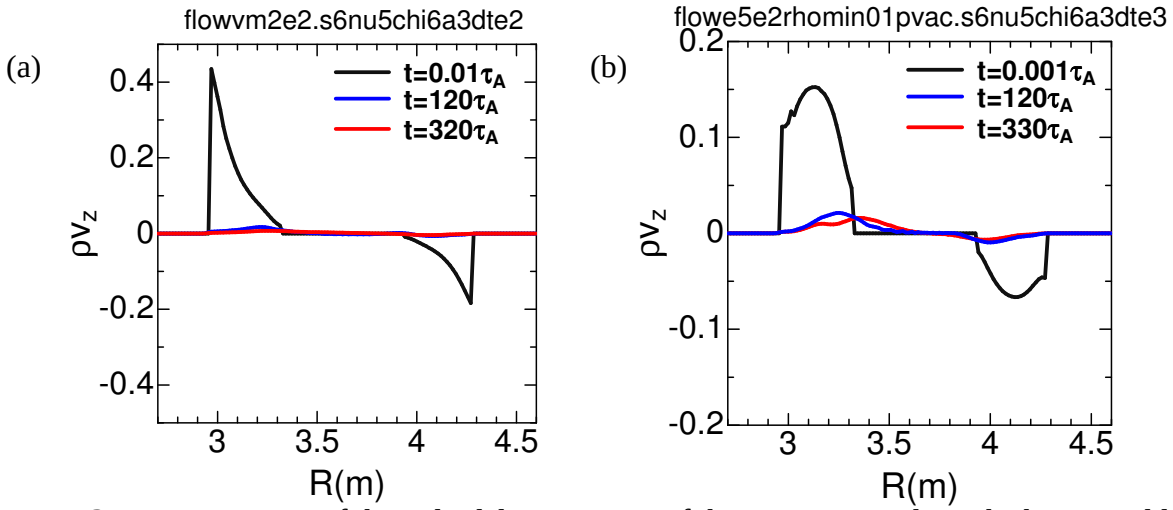

Figure 3: Time sequence of the poloidal component of the momentum along the horizontal line in the horizontally elongated cross section for (a) $\rho_{ini} = \rho_1$ and (b) $\rho_{ini} = \rho_2$.

surface with $\iota = 1$ exists in the plasma column. The Mercier index at the surface is $D_I = 1.5$, which indicates that the surface is strongly unstable against the interchange mode. The profiles of the flow components corresponding to Fig.1 (a) are also plotted. In the present study, we employ two types of the initial density ρ_{ini}, which are given by

$$\rho_1 = \rho_0 \text{ (=const.)} \quad \text{and} \quad \rho_2 = \rho_0[0.9(1-s^2)(1-s^3)+0.1]. \tag{2}$$

At first, $\rho_{ini} = \rho_1$ is employed. In the no flow case, the $m = 4/n = 4$ interchange mode linearly grows as is indicated by the value of D_I, and is saturated nonlinearly around $t = 300\tau_A$, where τ_A denotes the Alfvén time. As shown in Fig. 2 (a), a large amount of pressure collapses in the saturation phase. In the case where the flow corresponding to the experimental data is applied, the mode grows and is saturated in the way similar to the no flow case as shown in Fig.2 (b). In the case where the flow that has 200 times larger amplitude of the experimental data is applied, the pressure collapse is slightly reduced as shown in Fig.2 (c). These results show that the global flow that has the profile of the experimental data has a potential to stabilize the interchange mode. In order to investigate how effectively the flow interacts with the mode growth, we plot the time sequence of the total poloidal momentum. As shown in Fig.3 (a), the flow decays immediately in the time evolution of the mode. The maximum momentum value is 4.35×10^{-1} at $t = 0.01\tau_A$, 1.73×10^{-2} at $t = 120\tau_A$, and 7.21×10^{-3} at $t = 320\tau_A$. This means that the initial flow does not sufficiently affect the mode dynamics. This rapid decay of the flow is attributed to the viscous damping. Since $\rho_{ini} = \rho_1$ is employed, the momentum has a sharp gradient and the damping effect is strong at the plasma edge.

In order to avoid the sharp gradient of the momentum, we employ $\rho_{ini} = \rho_2$. As shown in Fig.4 (a) and (b), in the case where the flow corresponding to the experimental data is applied,

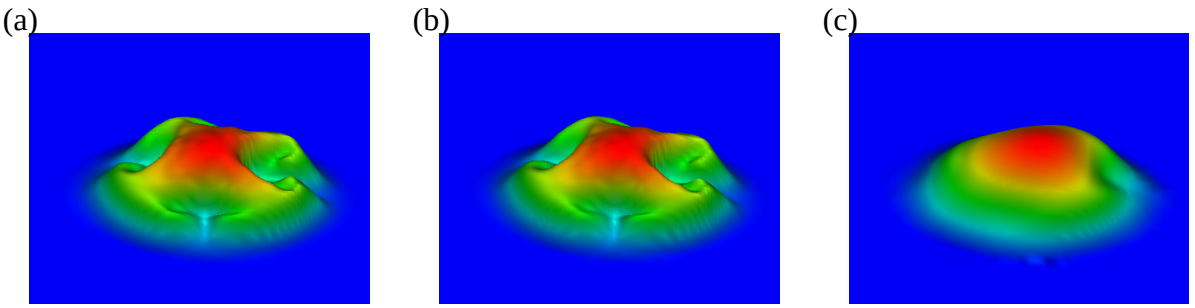

Figure 4: Total pressure profiles with the initial density $\rho_{ini} = \rho_2$ at t=330τ_A for the applied flows of (a) none, (b) $v_{\phi,exp}$ and $v_{Z,exp}$, and (c) $v_{\phi,exp} \times 500$ and $v_{Z,exp} \times 500$.

the pressure collapse similar to that in the no flow case occurs as well. In the case where the flow that has 500 times larger amplitude of the experimental data is applied, the pressure collapse is more reduced than that in the $\rho_{ini} = \rho_1$ case as shown in Fig.4 (c). In this case, the maximum momentum value is 1.52×10^{-1} at $t = 0.01\tau_A$, 2.14×10^{-2} at $t = 120\tau_A$, and 1.61×10^{-2} at $t = 330\tau_A$, as shown in Fig.3 (b). Note that the initial kinetic energy for Fig.4 (c) is less than that for Fig.2 (c). Thus, the larger momentum with $\rho_{ini} = \rho_2$ remains in the interaction with the mode growth compared with the case of $\rho_{ini} = \rho_1$, however, the survival fraction is still small.

4. Summary

The numerical scheme for the calculation of the global flow consistent with the experimental data has been established. By utilizing the scheme, we obtain the 3D flow profile in the whole plasma region from the 1D observed data. The results of the dynamics study of the flow effect on the interchange mode show that the flow obtained with this scheme has a stabilizing contribution. However, in the constant initial density case, the flow decays rapidly because of the viscosity before the mode substantially grows. Therefore, the interaction is not considered to be incorporated appropriately. To avoid the rapid flow decay, the density profile that drops at the edge is introduced, however the improvement is still limited. Adding a source term corresponding to the viscous decay of the flow to the momentum equation would be useful in future.

References

[1] S. Sakakibara, et al., . Nucl. Fusion, **53**, (2013) 043010.

[2] Y. Suzuki, et al., Nucl. Fusion **46** L19 (2006).

[3] Y. Todo, et al,. Plasma and Fusion Res. **5** S2062 (2010).

[4] K. Ichiguchi, et al., Plasma and Fusion Res. **11**, 2403035 (2016).

[5] K. Ichiguchi, et al., Proc. 26th IAEA Fusion Energy Conference, Kyoto, (2016).

[6] S. P. Hirshman, et al., Comp. Phys. Comm. **43** 143 (1986).